Modelling the energy dependent X-ray variability of Mrk 335

K. Akhila^a, Ranjeev Misra^b, Rathin Sarma^c, Savithri H. Ezhikode^{d,e}, K. Jeena^a

^aDepartment of Physics, Providence Women's College (Autonomous), University of Calicut, 673009, Kerala, India ^bInter-University Centre for Astronomy and Astrophysics (IUCAA), PB No.4, Ganeshkhind, Pune, 411007, India ^cDepartment of Physics, Rabindranath Tagore University, Hojai, 782435, Assam, India ^dSt. Francis de Sales College (Autonomous), Electronics City, Bengaluru, 560100, India ^eDepartment of Physics and Electronics, CHRIST (Deemed to be University), Bangalore, 560029, India

Abstract

We present a technique which predicts the energy dependent fractional r.m.s for linear correlated variations of a pair of spectral parameters and apply it to an XMM-Newton observation of Mrk 335. The broadband X-ray spectrum can be interpreted as a patchy absorber partially covering the primary emission, a warm and hot coronal emission or a relativistically blurred reflection along with the primary emission. The fractional r.m.s has a non-monotonic behavior with energy for segments of lengths 3 and 6 ksecs. For each spectral model, we consider every pair of spectral parameters and fit the predicted r.m.s with the observed ones, to get the pair which provides the best fit. We find that a variation in at least two parameters is required for all spectral interpretations. For both time segments, variations in the covering fraction of the absorber and the primary power law index gives the best result for the partial covering model, while a variation in the normalization and spectral index of the warm component gives the best fit in the two corona interpretation. For the reflection model, the best fit parameters are different for the two time segment lengths, and the results suggests that more than two parameters are required to explain the data. This, combined with the extreme values of emissivity index and reflection fraction parameters obtained from the spectral analysis, indicates that the blurred reflection model might not be a suitable explanation for the Mrk 335 spectrum. We discuss the results as well as the potential of the technique to be applied to other data sets of different AGN.

Keywords: X-rays:galaxies, galaxies:Seyfert, methods:numerical, galaxies:individual:Mrk 335

1. Introduction

Studying the X-ray emission is one way to understand the physics of the inner mechanisms in active galactic nuclei (AGNs). A long known property of AGN emission is the Xray flux variability. Long term variabilities, spanning from a few days to years, were first identified with the Ariel 5 and HEAO 1 missions (e.g., Marshall et al. 1981). Short rapid variabilities of the order of thousands of seconds were identified much later through missions such as EXOSAT (e.g., McHardy 1985). In the 0.1 - 10 keV band, flux variations are observed on timescales scanning a wide range from a few thousand seconds to years, having amplitude variations upto an order of magnitude (McHardy, 1988; Green et al., 1993; Turner, 1994; Turner et al., 1999).

A multitude of studies have been conducted on the AGN X-ray flux variabilities (Lawrence et al., 1987; Lawrence and Papadakis, 1993; Nandra, 2001; Martin Gaskell and Klimek, 2003; Markowitz et al., 2003; Soldi et al., 2014; Pryal et al., 2015; Komossa et al., 2016; Papadakis and Binas-Valavanis, 2024; Serafinelli et al., 2024). One way of quantifying the variability is through statistical tools such as excess variance and fractional rms variability amplitude (F_{var} : Vaughan et al.

2003). These quantities are estimated after removing the contribution from measurement errors and are hence an indicator of the intrinsic variability of the source.

The X-ray spectra of a typical Seyfert galaxy exhibits a power law emission along with the presence of broad and narrow emission lines (Fabian et al., 2000; Tatum et al., 2012). At low energies (< 2 keV) the flux from the power law emission is enhanced by another smooth component, known as the soft excess. It was first observed in the year 1985 by Singh et al. (1985) in the Seyfert-1 galaxy Mrk 509 and by Arnaud et al. (1985) in Mkn 841 using HEAO and EXOSAT observations, respectively. The soft excess has since been observed in several Narrow Line Seyfert-1 (NLS1) galaxies (Boller et al., 1995; Bühler et al., 1995; Middleton et al., 2007; Middei et al., 2019; Boller, 2023). Soft excess refers to an additional emission in the soft X-ray energies of these AGNs, which cannot be explained by the low-energy extrapolation of their hard energy continuum (Done and Nayakshin, 2007; Done et al., 2012; Middei et al., 2020). Observations have revealed the presence of soft excess in both broad and narrow line Seyfert-1 galaxies, but with a stronger strength in NLS1 galaxies (Gliozzi and Williams, 2020).

Several different theoretical models including the obscured model, warm coronal picture and a gravitational blurred reflection model have been used to explain the soft excess. Despite the crucial differences in their underlying physics, all these pro-

posed models were quite successful in explaining the observed spectrum (Sobolewska and Done, 2005; Ding et al., 2022). The partial covering model describes the excess as a 'leakage' through a non-uniform absorber. The power law continuum is obscured by the absorber. The presence of such patchy clouds, introduce variations in spectral behavior, waning a fraction of the incident radiation. Both this obscured emission and direct primary emission contribute to the observed spectrum. The changes in spectral features may then be attributed to changing line-of-sight absorber, without requiring alterations in the primary emitter. (Weaver et al., 1993; Tanaka et al., 2004; Grupe et al., 2008; Reeves et al., 2008; Gallo et al., 2011, 2015; Iso et al., 2016; Tripathi et al., 2019; Parker et al., 2019; Komossa et al., 2020). Several studies, including earlier ones like Weaver et al. (1993) and Turner et al. (1996), use the partial covering model to explain the X-ray spectra of Seyfert galaxies (Chevallier et al., 2006; Middleton et al., 2007). In the warm thermal Comptonization picture, there is an optically thick warm corona which is distinct from the hot corona. The seed photons from the far ultraviolet end of the accretion disk undergo Compton upscattering by warm (~ 0.1 keV) electrons in the corona giving rise to heightened emissions at low X-ray energies. The hot corona is responsible for the power law emission at higher energies (Dewangan et al., 2007; Middleton et al., 2009; Done et al., 2012; Ezhikode et al., 2017; Petrucci et al., 2018; Kubota and Done, 2018; Ursini et al., 2020). A multiepoch, multi-instrument analysis on the Seyfert-1 galaxy Zw 229.015 by Tripathi et al. (2019) suggested that the smooth and featureless spectrum favors the Comptonization picture. García et al. (2019), on the other hand, argue that the parameters required for thermal Comptonization are physically incompatible with the conditions of a standard corona. They put forward the relativistic reflection model as a better description of the observation. This gravitationally smeared ionised reflection component is another popular candidate for the origin of the soft excess (Miniutti and Fabian, 2004; Crummy et al., 2006; Liebmann et al., 2018). It refers to the relativistic reflection from the innermost regions of the accretion disk. The X-ray continuum gets reflected from the accretion disk and is gravitationally blurred due to the close proximity of the black hole. Presence of soft reverberation lags also support the reflection model (Fabian et al., 2009; Alston et al., 2020). The reflection model has an additional advantage that it paves a way to understand the accretion mechanism in NLS1 galaxies (Reynolds, 2021). However, a study by Adegoke et al. (2017) showed that both the models are statistically similar in explaining the soft X-ray excess. Another recent XMM-Newton study on a sample of six NLS1 galaxies by Yu et al. (2023) also gives a similar result. They confirm the presence of a warm and optically thick corona in the Comptonization model while reflection picture is a better explanation for the behaviour of single source.

In this work, we present a technique to model the source's energy dependent X-ray variability and recognise the parameters causing the variability for all spectral models. We determine the observed fractional rms (F_{var}) as a function of energy from the source lightcurves extracted in multiple energy bands. The different spectral models may then be used to predict the

fractional rms. The X-ray variability is attributed to a pair of spectral parameters, varying in correlation, from which, F_{var} is then predicted and the parameter pair that best recreates the observed temporal variation is identified. We demonstrate the method by an investigation of the X-ray spectrum of Markarian 335 (Mrk 335).

Mrk 335 is one of the widely studied Seyfert-1 galaxies (Longinotti et al., 2007; Grupe et al., 2008; Tombesi et al., 2010; Liu and Wang, 2010; Patrick et al., 2011; Longinotti et al., 2013; De Marco et al., 2013; Kara et al., 2013; Wilkins et al., 2015; Sarma et al., 2015; Chainakun and Young, 2015; Epitropakis et al., 2016; Chainakun et al., 2016; Emmanoulopoulos et al., 2016; Choudhury et al., 2019; Ingram et al., 2019; Ezhikode et al., 2021; Liu et al., 2021b,a; Yang et al., 2022; Hancock et al., 2022). It harbours a supermassive black hole of mass ~ $2.6 \times 10^7 M_{\odot}$ (Grier et al., 2011). Its X-ray spectrum resembles that of a typical NLS1 galaxy. It exhibits a very strong soft excess and prominent iron lines (O'Neill et al., 2007; Larsson et al., 2008). The soft excess in Mrk 335 was first observed in 1987 and has since been extensively observed (Pounds et al., 1987; Turner and Pounds, 1988). Mrk 335 has been observed to be variable in X-ray (Arévalo et al., 2008; Gallo et al., 2018) and we make use of this variability to understand the origin of the soft excess in the source.

This paper is organised as follows. The details of observation and data reduction techniques employed are given in Section 2. Section 3 explains the different ways in which the source's X-ray spectrum was modelled. In Section 4, F_{var} determination and rms spectrum are explained. In Section 5, the method used for predicting F_{var} from theoretical models is detailed. Finally we discuss the results in Section 6.

2. Observations and Data Reduction

ESA's *XMM-Newton* Observatory (Jansen et al., 2001) has observed Mrk 335 several times since 2000. The source was observed to have fallen into a state of very low flux in 2007 (Grupe et al., 2007; Longinotti et al., 2008) and has continued to remain so with occasional flaring episodes. For our analysis, we selected a ~ 133 ks long observation made in 2006 (Obs Id 0306870101, PI: Nandra) while the source was still in its brightest stage and showed large variability.

We consider the epic-pn camera (Strüder et al., 2001) data alone for the analysis. The data was processed using the Science Analysis Software sas-20.0.0. Following the standard procedures, the data was first filtered to remove the high background flares. sas tool tabstigen was used to set the threshold value for the count rates and a file containing the good time intervals (GTI) was created. Data with the conditions PATTERN≤4 and FLAG==0 only were selected. The task EPATPLOT was used to verify that the observation was free from pileup. X-ray spectrum was extracted from a central circular region of radius 35". The sas tasks RMFGEN and ARFGEN were used to generate the response matrix and auxiliary response files respectively. The task specgroup was used and the spectrum was grouped to have a maximum of three bins per resolution FWHM, with a minimum of 30 counts in every bin. Spectral

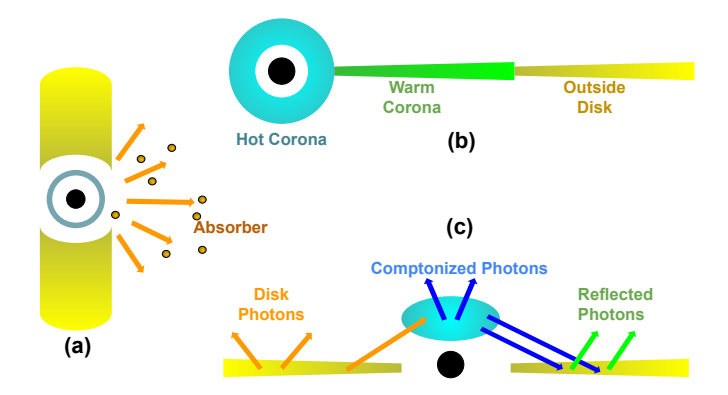


Figure 1: (a): Patchy absorber partially covering the primary emission. (b): Thermal Comptonization model geometry, where the disk (yellow) photons enter the warm Comptonization region (green) and then a fraction of these photons from warm corona enter the hot corona (blue). (c): Blurred reflection model, wherein the corona (blue) illuminates a portion of the accretion disk (yellow). The coronal geometry maybe of different flavors like the lamppost model, spheroidal or toroidal corona or the sandwich model.

fitting was done using the XSPEC-12.12.0 tool (Arnaud, 1996) of HEASOFT. Lightcurves were extracted with a time bin size of 100 s from a central source region of size 35". EPICLCORR was used to subtract background lightcurves extracted from a region of the same size and to account for dead time and exposure variations.

3. Spectral Analysis

Spectral fitting was done for the epic-pn X-ray spectrum in the 0.3 – 10.0 keV energy band. The xspec tool uses the χ^2 statistic to perform the fit. We obtain the errors from XSPEC, which gives their 90% confidence interval. The X-ray spectrum was a power law continuum overlaid by emission lines. Prominent emission lines were seen in the iron band at 6.4 - 7.0 keVand were fit with Gaussian (zgauss) components. These correspond to the neutral Fe $K\alpha$ emission line at ~ 6.4 keV and ionised Fe xxvi line at ~ 7.0 keV (O'Neill et al., 2007). Cosmological redshift for the source was taken to be z = 0.02578(Huchra et al., 1999) and the Galactic absorption (N_H) was fixed at $3.56 \times 10^{20} cm^{-2}$ (Kalberla et al., 2005). Previous studies have revealed a significant presence of warm absorber zones in the source spectra (Gallo et al., 2013). Hence we added two absorption edges at low energies which improved the spectral fitting. The observed soft X-ray excess of the source has been a subject of detailed analysis (Grupe et al., 2008; Brightman and Nandra, 2011; Zhong and Wang, 2013; Parker et al., 2014; Gallo et al., 2015; Wilkins and Gallo, 2015; Keek and Ballantyne, 2016; Boissay et al., 2016). These analyses demonstrate that the broadband X-ray spectrum can be described by a partial covering model, as a Compton upscattering of the seed photons or by a relativistic reflection model. We fit the spectrum accordingly.

3.1. Model-I: Partial Covering Model

In the partial covering scenario, the intrinsic continuum emission of the source is modified by a partially covering absorber.

In this model, the spectrum is described with the absorber reshaping the underlying single power law. We follow the spectral model prescribed in Grupe et al. (2008), for the same observation. Partial covering of the primary emission is achieved by applying the zpcfabs component to power law. This absorber model gives a better fit on adding Gaussian components of widths 0.25 keV, that mimic line emission for the soft emission lines. Additionally, we added an absorption edge at 0.42 keV, which improved the fit. The two soft energy Gaussians are added at energies ~ 0.1 keV and ~ 0.8 keV. We obtained a continuum power law index of 2.31. The column density for the partial covering absorber is $N_{H,pc} = 45.77 \times 10^{22} \ cm^{-1}$ with a covering fraction of 0.46. We obtained a fit statistic of $\chi^2/\text{d.o.f.}$ = 302.3/163. While this value is on the higher side, we note that, following the data grouping adopted in Grupe et al. (2008), we obtained a χ^2 /d.o.f = 917.4/700, closer to the reduced χ^2 of 1.2 in Grupe et al. (2008). The spectral fitting plot is shown in Figure 2a and the parameters of fit are listed in Table 1.

3.2. Model-II: Thermal Comptonization

Here, the X-ray continuum was modeled as Comptonized emission of the seed photon spectrum. The seed photons are Compton upscattered by the hot electrons in the corona resulting in an enhanced emission at low energies. As already discussed in Section 1, in this model, the soft X-ray excess is considered to be due to the warm coronal component (Porquet et al., 2018; Middei et al., 2018; Noda and Done, 2018; Matzeu et al., 2020). Such a two component model can have a geometry where the two occupy physically different regions. Here, the warm corona is connected to the accretion disk, while the hot corona lies beyond (Figure 1). We consider the case where the UV disk photons enter the warm Comptonizing region first and then the photons from the warm coronal medium enter the hot corona (Ezhikode et al., 2016; Kubota and Done, 2018; Zoghbi and Miller, 2023). Warm corona Comptonizes the disk photons, giving the soft emission and a fraction of these photons are further scattered by the hot corona and emit in the hard X-ray energies. We use two xspec models, namely simpl and nthComp, to represent the hot and warm components, respectively. The disk photons enter the warm corona represented by nthComp emitting in the soft region, while a fraction of this is further upscattered by the hot corona represented by simpl, an empirical model for the Comptonization of a fraction of seed photons to a higher temperature (Steiner et al., 2009). The seed photons were considered to be blackbody in shape (inp_type=0). The spectral fitting plot is shown in Figure 2b. We obtained a photon index (Γ_{simpl}) value of \sim 1.82. The seed photon temperature obtained was $\sim 5.98 \times 10^{-2}$ keV. The spectral fit gives a value of 0.98 keV for the electron temperature. While we were unable to obtain a constraint on its upper limit, the parameter had a lower limit of 0.69 keV. A complete list of the parameters of fit is given in Table 2.

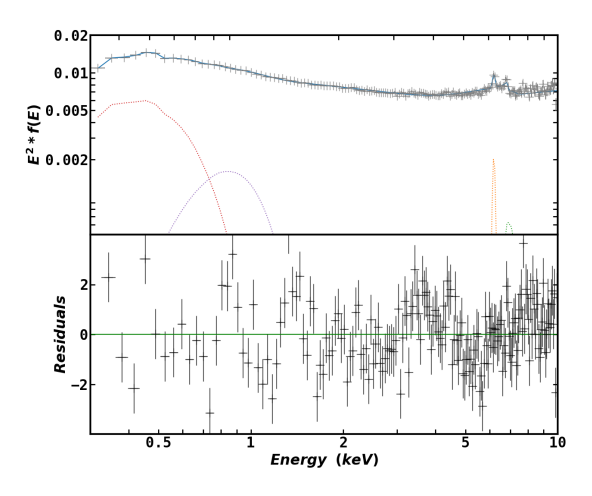
3.3. Model-III: Relativistic Reflection

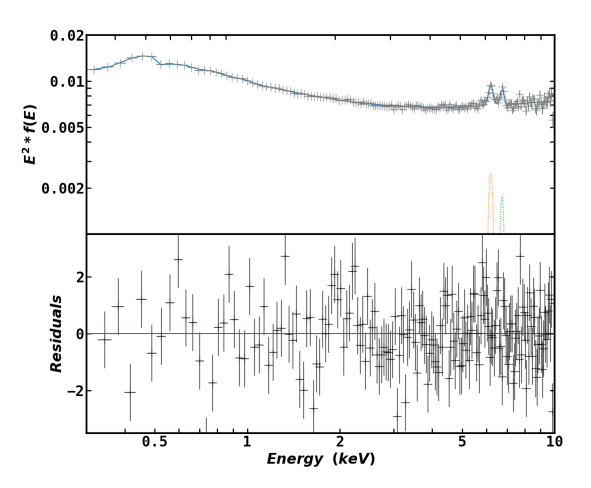
In this case, the spectrum was modelled as a standard relativistic reflection model. Blurred reflection features arise in the

Table 1: Spectral parameters for Model-I in the energy range 0.3 – 10.0 keV.

Model	Parameter	Value	
zedge	E (keV)	$0.42^{+0.006}_{-0.005}$	
	au	$0.16^{+0.02}_{-0.02}$	
zpcfabs	$N_{H,pc} (\times 10^{22})$	$45.77_{-6.06}^{+7.05}$	
	f_c	$0.46^{+0.03}_{-0.03}$	
powerlaw	Γ_{pl}	$2.31^{+0.01}_{-0.01}$	
	$N_{pl}(\times 10^{-2})$	$1.80^{+0.11}_{-0.10}$	
zgauss1	$E_l(\text{keV})$	0.10 (frozen)	
	N	$0.15^{+0.01}_{-0.01}$	
zgauss2	$E_l(\text{keV})$	$0.76^{+0.01}_{-0.01}$	
	$N(\times 10^{-3})$	$3.23^{+0.30}_{-0.26}$	
zgauss3	$E_l(\text{keV})$	$6.41^{+0.03}_{-0.03}$	
	$\sigma(\text{keV})$	< 0.12	
	$N(\times 10^{-5})$	$1.16^{+0.38}_{-0.34}$	
zgauss4	$E_l(\text{keV})$	$7.17^{+0.17}_{-0.14}$	
	$\sigma(\text{keV})$	0.25 (frozen)	
	$N(\times 10^{-5})$	$1.16^{+0.43}_{-0.44}$	
χ^2/dof		302.3/163	

spectrum when the 'cold' accretion disk is illuminated by the 'hot' corona. Since the disk efficiently radiates, it is colder than the coronal material. The geometry of this hot corona is still not properly understood, however, some possibilities discussed in literature are the lamppost model, spheroidal or toroidal corona and the sandwich model. A fraction of the photons from the corona can illuminate the disk, giving rise to the reflection spectrum (Bambi, 2024). The relxill code (Dauser et al., 2014; García et al., 2014; Dauser et al., 2016, 2020) was used to model the complex relativistically blurred reflection component. It offers two variations, the lamppost geometry (relxilllp, relxilllpCp) and the coronal geometry (relxill, relxillCp). For our analysis, we use the coronal model for a Comptonization continuum (relxillCp, Figure 1). It accounts for the gravitationally blurred reflection of the Comptonization continuum from the accretion disk. The spin parameter, a, was fixed at 0.998 which is its maximal allowed value. The two indices were tied together while the break (R_{br}) and outer (R_{out}) radii were fixed at $300R_g$ and $400R_g$, respectively. The calculations were done for a fixed accretion disk density of $10^{15} cm^{-3}$ and a coronal electron temperature of 60 keV. The corresponding X-ray fitting plot is shown in Figure 2c. The power law index for the incident spectrum (Γ_{relx}) obtained was ~ 2.20 while the reflection fraction was ~ 9.49 . Ionization parameter ($log\xi$) returned a value of ~ 2.70. Inner radius (R_{in}) lies between $1 - 1.1R_{ISCO}$. Emissivity profile is defined by $r^{-Index1}$ and $r^{-Index2}$ between R_{in} & R_{br} and R_{br} & R_{out} , respectively. These two parameters were tied together. We obtained a lower limit of 8.30 for Index1, the parameter has an upper limit of 10 in the model. This agrees with the steep emissivity profiles, with index values greater than 5, previously been observed for Mrk 335 (Gallo et al., 2013; Wilkins et al., 2015; Gallo et al., 2019). Table 3 lists all the parameters of fit.





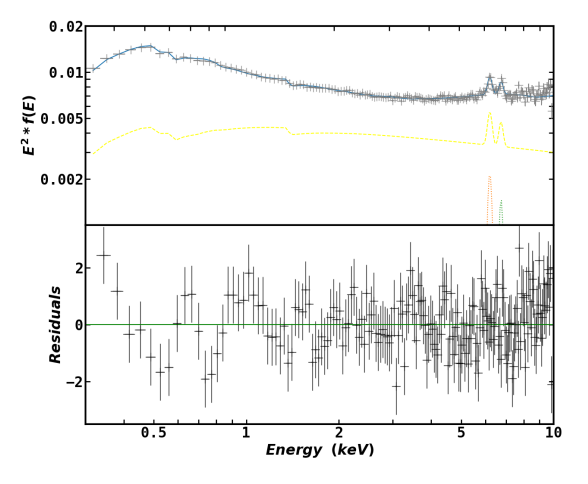


Figure 2: X-ray spectral fitting of epic-pn observation in the energy range 0.3 – 10.0 keV. Spectral fitting using the three models namely, partial covering model (Model-I, top row), the thermal Comptonization model (Model-II, middle row) and the blurred reflection model (Model-III, bottom row), respectively are shown. In all figures, dotted lines represent the individual additive components in the model.

Table 2: Spectral parameters for Model-II in the energy range 0.3 – 10.0 keV.

Component	Parameter	Value	
zedge1	E_c (keV)	$0.38^{+0.01}_{-0.02}$	
	au	$0.17^{+0.098}_{-0.058}$	
zedge2	E_c (keV)	$1.12^{+0.03}_{-0.03}$	
	au	$0.029^{+0.008}_{-0.009}$	
zgauss1	E_l (keV)	$6.41^{+0.03}_{-0.03}$	
	σ	0.1(frozen)	
	$N(\times 10^{-5})$	$1.68^{+0.220}_{-0.217}$	
zgauss2	E_l (keV)	$6.96^{+0.04}_{-0.04}$	
	σ	0.1(frozen)	
	$N(\times 10^{-5})$	$1.00^{+0.208}_{-0.207}$	
simpl	Γ_{simpl}	$1.82^{+0.03}_{-0.15}$	
	f	$0.10^{+0.02}_{-0.04}$	
	UpScOnly	1.0(frozen)	
nthComp	Γ_{nthC}	$3.21^{+0.05}_{-0.05}$	
	kT_e (keV)	> 0.69	
	kT_{bb} (keV)	$0.0598^{+0.003}_{-0.005}$	
	$N_{nthC}(\times 10^{-3})$	$7.62^{+1.38}_{-0.57}$	
χ^2/dof		228.52/163	

Table 3: Spectral parameters for Model-III in the energy range 0.3 – 10.0 keV.

Component	Parameter	Value
zedge1	$E_c(keV)$	$0.62^{+0.02}_{-0.03}$
	au	$0.18^{+0.05}_{-0.04}$
zedge2	$E_c(keV)$	$1.47^{+0.04}_{-0.04}$
	au	$0.11^{+0.02}_{-0.02}$
relxillCp	i(deg)	$74.11^{+1.20}_{-2.49}$
	$R_{in}(R_{ISCO})$	< 1.1
	Index1	> 8.30
	Γ_{relx}	$2.20^{+0.01}_{-0.01}$
	$log \xi$	$2.70^{+0.06}_{-0.06}$
	A_{Fe}	$0.67^{+0.07}_{-0.07}$
	R_f	$9.495^{+3.01}_{-1.39}$
	$N_{relx}(\times 10^{-5})$	$5.597^{+0.40}_{-0.62}$
zgauss1	$E_l(keV)$	$6.41^{+0.03}_{-0.03}$
	σ	0.1(frozen)
	$N(\times 10^{-5})$	$1.43^{+0.241}_{-0.252}$
zgauss2	$E_l(keV)$	$6.96^{+0.05}_{-0.04}$
	σ	0.1(frozen)
	$N(\times 10^{-6})$	$8.18^{+2.23}_{-2.45}$
χ^2/dof		167.6/161

4. Fractional Variability and RMS Spectra

Fractional variability is a useful tool for studying the variability properties of AGNs in different energy ranges. The statistical quantity, fractional root mean square variability amplitude, F_{var} , is defined as the square root of normalised excess variance (Edelson et al., 1990; Rodriguez-Pascual et al., 1997). Excess variance is an indicator of the 'intrinsic' variability of the source in the sense that it is calculated after removing the effect of uncertainties (Edelson et al., 2002).

Fractional rms variability amplitude was determined following the method explained in Vaughan et al. (2003). F_{var} is defined as given by equation 1 (Eqn. 10 of Vaughan et al. (2003)) .

$$F_{var} = \sqrt{\frac{S^2 - \overline{\sigma_{err}^2}}{\bar{x}^2}} \tag{1}$$

where S is the sample variance given by equation 2 (Eqn. 6 of Vaughan et al. (2003)):

$$S^{2} = \frac{1}{N-1} \sum_{i=1}^{N} (x_{i} - \bar{x})^{2}$$
 (2)

and $\overline{\sigma_{err}^2}$ is the mean square error as given by equation 3 (Eqn. 9 of Vaughan et al. (2003)):

$$\overline{\sigma_{err}^2} = \frac{1}{N} \sum_{i=1}^{N} \sigma_{err,i}^2$$
 (3)

The error on F_{var} is given by Eqn. B2 of Vaughan et al. (2003). We extracted light curves in multiple energy bins. For each lightcurve we consider segments of different lengths, giving us segments of sizes, 500 secs, 700 secs, 1 ks, 1.5 ks, 3 ks and 6 ks. For each case average count, variance and excess variance were calculated at all energy bins, from which F_{var} and its errors were determined using the above equations. We denote the F_{var} values, thus estimated from the observation, by F_0 . The rms spectra for this observation was then created by plotting F_0 as a function of energy. We find that for segment sizes lower than 3 ks, for some of the energy bins, the excess variances were not detected. Hence we limit the analysis to segments of sizes 3.0 and 6.0 ks. Figure 3 plots the rms spectra for the 3 and 6 ks segments.

5. Fractional Variability Prediction

5.1. Method

We ascribe the variation of the count rate at a certain energy band, R_i (where the subscript i denotes the energy band) being caused by variations in the values of two spectral parameters, X and Y. In the linear approximation this implies that the variation of the count rate, ΔR_i can be written as:

$$\Delta R_i(X,Y) = \left(\frac{\partial R_i}{\partial X}\right)_{X_0} \Delta X + \left(\frac{\partial R_i}{\partial Y}\right)_{Y_0} \Delta Y \tag{4}$$

where X_0 and Y_0 are the steady state values of X and Y and ΔX and ΔY are their variation. Noting the predicted normalised F_{var}

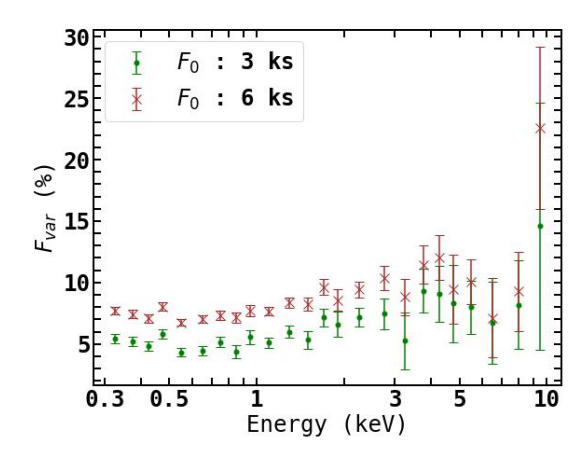


Figure 3: RMS spectra plotting the observed F_{var} as a function of energy. Source lightcurves were extracted at different energy bands. From each of those lightcurves, F_{var} were determined and plotted against energy. This was repeated for lightcurves with different segment sizes, 3 and 6 ks.

at the energy band denoted by *i* is F_{Pi} , given by, $F_{Pi}^2 = (\Delta R/R_i)^2$, this implies that :

$$F_{Pi}^{2} = A_{i}^{2} \delta X^{2} + B_{i}^{2} \delta Y^{2} + 2A_{i} B_{i} C_{XY} |\delta X| |\delta Y|$$
 (5)

where $\delta X = \Delta X/X_0$, $\delta Y = \Delta Y/Y_0$, $A_i = \frac{X_0}{R_i} \left(\frac{\partial R_i}{\partial X}\right)_{X_0}$ and $B_i = \frac{Y_0}{R_i} \left(\frac{\partial R_i}{\partial Y}\right)_{Y_0}$. C_{XY} represents both the strength and the sign of the cross term, such that $C_{XY} = 1, 0, -1$ represent the cases when the δX and δY are correlated, un-correlated and anti-correlated. Fractional values of C_{XY} can be either interpreted as when δX and δY are partially correlated or that there is a phase lag between them such that $C_{XY} = cos\phi$.

tween them such that $C_{XY} = cos\phi$.

The partial derivatives $\left(\frac{\partial R_i}{\partial X}\right)_{X_0}$ and $\left(\frac{\partial R_i}{\partial Y}\right)_{Y_0}$ were estimated numerically using the xspec software. We considered the best fit model spectra and then found the change in the model count rate at a given energy band by introducing a 10% variation in the value of the parameter. The ratio of this change in the count rate to that of the parameter value was taken as the partial derivative. Note that since this exercise was undertaken in the model count rates (and not the photon rate), the response of the instrument is being taken into account. The best fit spectra values were then used to estimate A_i and B_i .

The predicted F_p was then compared with the observed ones to obtain the best fit values for $|\delta X|$, $|\delta Y|$ and C_{XY} by minimising the chi-square function :

$$\chi^2 = \sum_{i=0}^n \left(\frac{F_{0i}^2 - F_{Pi}^2}{\sigma_i} \right)^2 \tag{6}$$

Here, F_{0i}^2 is the squared observed fractional rms variability amplitude (F_{var}) and σ_i is the error on F_{0i}^2 . We note that the minimisation of χ^2 can be done analytically and one can obtain expressions for the best fit values as shown in Appendix A. However, these analytical expressions sometimes gave unphysical best fit values such as $|\delta X|$ or $|\delta Y| < 0$ or $|C_{XY}| > 1$. Thus, we had to use the python library LMFIT (Newville et al., 2016),

to minimise the χ^2 which allows for the parameter values to be within a specified range.

5.2. Model-I: Partial Covering Model

To model the intrinsic variability, we consider the different spectral parameters. For a given segment size, the parameters were varied in combinations of one and two and all different combinations were considered. For each combination, the parameter values were varied slightly and the corresponding R_{0i} , R_{1i} and R_{2i} values were determined for all different energy bins. From these, A_i and B_i can be estimated as explained above. These values were then input into LMFIT along with corresponding F_{0i}^2 and σ_i values. The fit parameters δX^2 , δY^2 , C_{XY} and the result F_P were obtained as output. The combination that gives the best χ^2 fit was determined, under the conditions that neither δX^2 nor δY^2 can be negative and C_{XY} lies between -1 and +1. The predicted rms spectra for a given segment size and a given combination of model parameters can be created by plotting F_P as a function of energy.

The spectral parameters were varied individually and in pairs. For both segment sizes, the best fit was given by a combination of the covering fraction (f_c) and the power law photon index (Γ_{pl}) . For a segment length of 3 ks, the combination is obtained for δf_c of 5.93% and $\delta \Gamma_{pl}$ of \sim 2.14%. Similarly, for the 6 ks case, the lowest χ^2 is obtained again for δf_c and $\delta \Gamma_{pl}$ values of 8.86% and 2.43%, respectively. In both the cases, the two parameters are slightly correlated with C_{XY} values of \sim 0.3. Table 4 lists the parameter combinations with lowest χ^2 for three cases, all other combinations give higher values of χ^2 . For both the 3ks and 6ks cases, we plot a continuous curve by determining F_P values at very small energy bins (0.1 keV) using these fit parameter values. The resultant spectra are plotted in Figures 4a and 4b.

5.3. Model-II: Thermal Comptonization

For the thermal Comptonization model, we consider all possible parameters that determine the X-ray spectrum in the full energy range. As with the partial covering model, the parameters are varied individually and in combinations of two. We found that varying the electron temperature (kT_e) does not bring about a significant change in the count rates and hence was not considered during the analysis. The whole procedure was repeated for all combinations of the model parameters for both segment sizes. For the 3 ks case, we get the best fit by varying the parameters, photon index (Γ_{nthC}) and normalisation (N_{nthC}) of the warm corona. The values of $\delta\Gamma_{nthC}$ and δN_{nthC} are $\sim 2.49\%$ and $\sim 5.66\%$ respectively with a $C_{XY} \sim -0.59$, indicating a significant anti-correlation between the two parameters. For the case with a larger segment of 6 ks length, the best fit is again given by the combination of photon index (Γ_{nthC}) and normalisation (N_{nthC}) , with the values of $\delta\Gamma_{nthC}$ and δN_{nthC} being $\sim 2.87\%$ and $\sim 8.15\%$. In this case also, we see a slight correlation between the two parameters with $C_{XY} \sim -0.51$. Parameter combinations with the least values of χ^2 are listed in Table 5. The continuous curve is plotted for small energy bins of size 0.1 keV, as shown in Figures 4c and 4d.

Table 4: Fit statistics for different parameter combinations of Model-I.

Segment	X	δX	Y	δY	C_{XY}	χ^2/dof
Size		(%)		(%)		
	f_c	$5.93^{+0.20}_{-0.22}$	Γ_{pl}	$2.14^{+0.23}_{-0.25}$	$0.29^{+0.06}_{-0.06}$	17.89/21
3 ks	f_c	13.14	N_{pl}	14.39	0.91	22.15/21
	Γ_{pl}	1.97	N_{pl}	6.30	0.35	25.47/21
	f_c	$8.86^{+0.18}_{-0.16}$	Γ_{pl}	$2.43^{+0.22}_{-0.26}$	$0.28^{+0.05}_{-0.04}$	18.95/21
6 ks	f_c	15.47	N_{pl}	16.24	0.84	24.82/21
	Γ_{pl}	2.50	N_{pl}	9.37	0.45	39.83/21

Table 5: Fit statistics for different parameter combinations of Model-II.

Segment	X	δX	Y	δY	C_{XY}	χ^2/dof
Size		(%)		(%)		
	Γ_{nthC}	$2.49^{+0.26}_{-0.29}$	N_{nthC}	$5.66^{+0.19}_{-0.19}$	$-0.59^{+0.04}_{-0.04}$	16.93/21
3 ks	f	10.40	N_{nthC}	4.91	0.04	21.88/21
	Γ_{simpl}	2.29	N_{nthC}	5.37	-1.00	36.85/21
	Γ_{nthC}	$2.87^{+0.23}_{-0.30}$	N_{nthC}	$8.15^{+0.16}_{-0.16}$	$-0.51^{+0.03}_{-0.03}$	16.98/21
6 ks	f	10.21	N_{nthC}	7.34	0.17	24.70/21
	Γ_{simpl}	2.25	N_{nthC}	7.72	-0.81	53.34/21

5.4. Model-III: Relativistic Reflection

As was done with the previous models, here we consider all parameters that determine the spectrum, except the iron abundance. We find that the model count rates are not sensitive to changes in the inner disk radius (R_{in}) and hence was not considered for the analysis. The procedure as described earlier was followed and the rms spectrum was predicted. The power law photon index (Γ_{relx}) and the accretion disk's ionisation parameter $(log\xi)$ of relxillCp gives the best fit for the case of 3 ks long segment. Here the values of $\delta\Gamma_{relx}$ and $\delta log\xi$ obtained are $\sim 1.91\%$ and $\sim 2.64\%$ and the two have a C_{XY} value of ~ -0.49 . For the 6 ks case, the best fit is given by a different parameter combination, power law index (Γ_{relx}) and normalisation (N_{relx}) parameters of relxillCp. We saw that, in this case, the two parameters are anti-correlated with the values of $\delta\Gamma_{relx}$ and δN_{relx} being $\sim 1.53\%$ and $\sim 8.90\%$ and $C_{XY} < -0.53$. Parameter combinations giving the best χ^2 values are tabulated in Table 6. As before, a continuous curve was also plotted by choosing very small energy bins of 0.1 keV size. The rms spectra are shown in Figures 4e and 4f.

6. Results and Discussion

Mrk 335 has an X-ray spectrum resembling that of a typical Seyfert-1 galaxy with a strong soft excess, with significant flux variations in the X-ray band. Broadband X-ray spectrum of the

Table 6: Fit statistics for different parameter combinations of Model-III.

Segment	X	δX	Y	δY	C_{XY}	χ^2/dof
Size		(%)		(%)		
	Γ_{relx}	$1.91^{+0.12}_{-0.17}$	logξ	$2.64^{+0.10}_{-0.14}$	$-0.49^{+0.10}_{-0.08}$	22.81/21
3 ks	Γ	1.58	N_{relx}	6.50	-0.65	23.91/21
	R_f	6.57	N_{relx}	8.89	-0.92	30.93/21
	Γ_{relx}	$1.53^{+0.23}_{-0.33}$	N_{relx}	$8.90^{+0.21}_{-0.24}$	< -0.53	29.86/21
6 ks	$log\xi$	15.82	N_{relx}	24.44	-0.95	44.57/21
	R_f	7.44	N_{relx}	12.74	-1.00	46.76/21

source can be interpreted as a partial covering absorber modifying the power law, a warm thermal Comptonization component or as the gravitational blurred reflection off the accretion disk. We fit spectral models representing these interpretations to the *XMM-Newton* observation of Mrk 335 and find that the spectrum can be well represented by all the aforementioned models. The photons indices obtained for all three cases are well within the range of 1.8 - 2.5, typically observed for such galaxies (Nandra and Pounds, 1994; Page et al., 2005).

The *XMM-Newton* observation considered in this work has been reported to show high variability in its X-ray emission (Wilkins and Gallo, 2015; Mastroserio et al., 2020). We estimated the fractional rms amplitude, F_{var} , as a function of energy, E, for two different segments of lengths 3 ks and 6 ks. We developed a scheme which, for a given spectral model fit, would predict $F_{var}(E)$ as being caused by the coherent variation of two of the spectral parameters, enabling the identification of the spectral parameters responsible for the observed variability. As can be seen from Figures 3 and 4, F_{var} is not a constant with energy. There is evidence that F_{var} decreases from 0.3 keV to about 0.7 keV and rises for higher energies. Our analysis shows that none of the three models can explain the observed profile using a single parameter variation; which always results in a reduced χ^2 greater than 45/21.

The partial covering interpretation of the X-ray spectrum, involves a single power law emission along with a neutral patchy absorber that partially covers the source. To explain the observed variation of fractional rms with energy, the analysis undertaken here shows that a variation in the primary emission itself is warranted. This is manifested as the best fit requires a variation in the power law index (Γ_{pl}) . A previous study by Yamasaki et al. (2016) on IRAS 3224- 3809 shows that, rms variability over a time scale of ~ 1 day is explained by changing the partial covering fraction. From our analysis of Mrk 335 using the partial covering scenario, variations on smaller time scale is again explained by variations in the covering fraction (f_c) along with the photon index. The results are the same for both the segment sizes, of 3 ks and 6 ks, with similar values of χ^2 . In both the cases, the parameters are slightly correlated with a C_{XY} of ~ 0.3 .

In the warm Comptonization interpretation, a hot corona Comptonizes photons from the warm corona, with the latter giving rise to the soft excess. Thus a variation of the normalization of the warm Comptonization component (with other parameters being constant) will lead to an overall normalization change in the full spectrum, leading to F_{var} which is constant with energy. In this case, the rms analysis shows that there needs to be a variation of photon index of the warm Comptonization (Γ_{nthC}). Moreover, the variation of the normalization and Γ_{nthC} are anti-correlated with each other since the crosscorrelation C_{XY} turns out to be negative. Note that Γ_{nthC} depends on the optical depth and temperature of the warm corona. A decrease in Γ_{nthC} implies an increase in the warm corona temperature or optical depth. Thus, the analysis suggests that the energy dependent F_{var} for both time-scales can be explained in terms of variations of the normalization and temperature (or optical depth) of the warm corona. It is interesting to note that

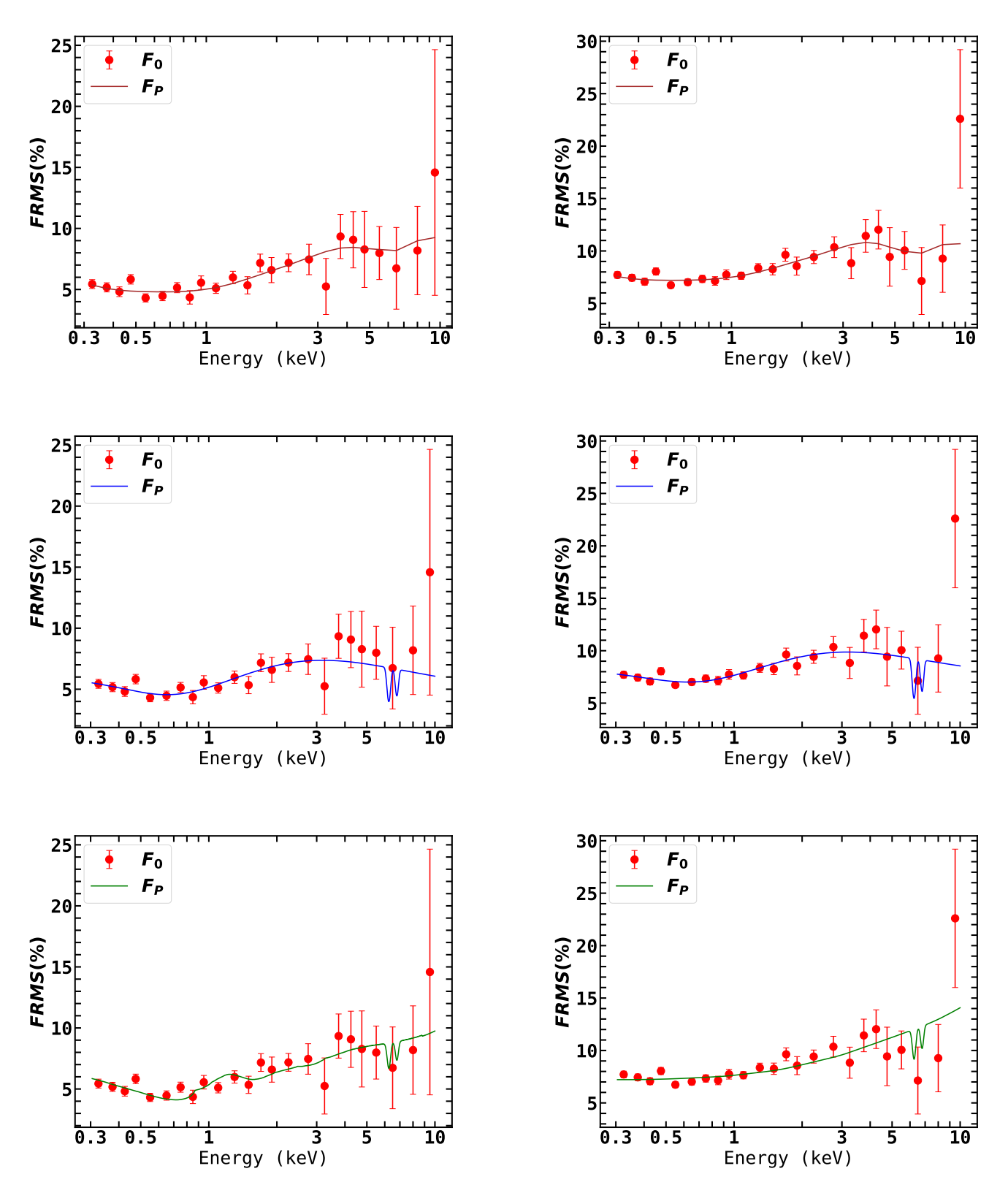


Figure 4: The observed F_{var} values (F_0) are plotted along with a continuous curve corresponding to the predicted F_{var} (F_P) using all the three models. Left and right panels show the plots for segment sizes 3 ks and 6 ks, respectively. From the top, F_P is predicted using the partial covering model (brown curve), warm Comptonization (blue curve) and blurred reflection (green curve), respectively.

although there is significant variability at high energies, the energy dependent F_{var} can be explained solely due to variations of the warm corona parameters, which changes the seed photons of the hot Comptonization component.

For the case when the soft excess is explained by the reflection component, we note the exceptionally high values of the emissivity index and the reflection fraction parameter. For this spectrum, a variation in the normalization of the reflection component will give rise to a constant energy independent F_{var} . The r.m.s. analysis shows that if combined with a change in the photon index Γ_{relx} , this leads to an increase in F_{var} with energy which can broadly explain the data as shown in Figure 4f (segment size of 6 ks). However, this does not produce the dip in F_{var} at ~ 0.7 keV, leading to a higher value of $\chi^2/dof = 30/21$ (Table 6). It is interesting to note that a combination of variations in photon index Γ_{relx} and ionization parameter $\log \xi$ can produce such a dip as seen for the fitting for segment size of 3 ks (Figure 4e). The same combination does not provide a good fit when the segment size is 6 ks resulting in $\chi^2/dof = 47.92/21$. This suggests that perhaps more than two parameter variation are required to explain the data. The steep emissivity profile and an extreme value of the reflection parameter for a non-pointlike X-ray source, combined with a requirement for variations in more than two parameters, indicates that the blurred reflection model might not be a suitable description of the Mrk 335 spectrum.

We note that the fit statistics are somewhat low for a few of these combinations, especially in the partial covering and the Comptonization models. Such low values of χ^2 suggests an over estimation of errors. This could possibly arise when there is an intrinsic correlation between the variabilities in different energy bands (Ingram, 2019). They stipulate the use of new formulae for calculating the errors in such situations, assuming that the variability power spectrum is known. However in our current case, the data is not sufficiently long enough for such detailed analysis. Furthermore it's not clear how to take this effect into account when the F_{var} is being computed directly from the lightcurve rather than power spectrum analysis.

The method prescribed here, attributes the X-ray variability to be caused by two spectral parameters varying in combination. It may also be possible that the system is indeed more complex and more than two parameters maybe varying. More detailed modelling taking into account the physical dependence of the spectral parameters on each other is required to make more concrete conclusions. Moreover, the results depend on the specific spectral model used to fit the energy spectrum. More sophisticated spectral models such as those which compute the emissivity index self consistently for a specific geometry (e.g. the relxilllp, for the 'lamp-post' model) and incorporating complex absorption models to account for the observed edges may be required. Nevertheless, the method presented in this work, has the potential to differentiate between spectrally degenerate models. Moreover, the work needs to be extended to other data sets especially at high energies (perhaps using NuStar observations) to complement the results presented here.

Acknowledgements

Authors KA and KJ acknowledge the financial support from ISRO (Sanction Order:No.DS_2B-13013(2)/11/2020-Sec.2). KA thank the IUCAA visiting program. KJ and RS acknowledge the associateship program of IUCAA, Pune. This research has made use of data, software and/or web tools obtained from the High Energy Astrophysics Science Archive Research Center (HEASARC), a service of the Astrophysics Science Division at NASA/GSFC and of the Smithsonian Astrophysical Observatory's High Energy Astrophysics Division.

Appendix A. Analytical solution for fit parameters of predicted fractional variability

The parameters δX^2 , δY^2 and C_{XY} in Eqn. 5 may also be determined analytically. This makes use of the function χ^2 defined by Eqn. 6. For the cases,

$$\frac{d\chi^2}{d\delta X^2} = 0 \quad \frac{d\chi^2}{d\delta Y^2} = 0 \quad \frac{d\chi^2}{dC_{xy}} = 0$$
 (A.1a-c)

The set of equations given below follows directly

$$\begin{bmatrix} \sum_{i} \frac{A_{i}^{4}}{\sigma^{2}} & \sum_{i} \frac{A_{i}^{2} B_{i}^{2}}{\sigma^{2}} & \sum_{i} \frac{A_{i}^{2} B_{i}^{2}}{\sigma^{2}} \\ \sum_{i} \frac{A_{i}^{2} B_{i}^{2}}{\sigma^{2}} & \sum_{i} \frac{B_{i}^{2}}{\sigma^{2}} & \sum_{i} \frac{A_{i}^{2} B_{i}^{2}}{\sigma^{2}} \end{bmatrix} \begin{bmatrix} \delta X^{2} \\ \delta Y^{2} \\ C_{XY} \end{bmatrix} = \begin{bmatrix} \sum_{i} \frac{F_{0i}^{2} A_{i}^{2}}{\sigma^{2}} \\ \sum_{i} \frac{F_{0i}^{2} B_{i}^{2}}{\sigma^{2}} \\ \sum_{i} \frac{F_{0i}^{2} A_{i} B_{i}}{\sigma^{2}} \end{bmatrix}$$
(A.2a-c)

The equations A.2a-c can then be solved for δX , δY and C_{XY} respectively. If the term $\sum\limits_{i=0}^{n}\frac{1}{\sigma^2}A_i^2B_i^2$ was denoted as $A_i^2B_i^2$ and so on, then the equations become :

$$X^{2} = \frac{((F_{0}^{2}A_{1}^{2})(A_{1}^{2}B_{1}^{2}) + (F_{0}^{2}A_{1}^{2}B_{1}^{2})($$

 $\delta Y^2 = \frac{([F_0^2] \rho_i^2] \wedge (A_i^2) (A_i^2 B_i^2) + (F_0^2 A_i^2) (A_i B_i^2) + (F_0^2 A_i B_i) (A_i^2 B_i) - (F_0^2 A_i B_i) (A_i^2 B_i) + (F_0^2 A_i^2) (A_i^2 B_i^2) + (F_0^2 A_i^2 B_i) (A_i^2 B_i^2) + (F_0^2 B_i^2) (A_i^2 B_i^2) + (F_0^2 B_i^2) (A_i^2 B_i) (A_i^2 B_i^2) + (A_i^2 B_i^2) (A_i^2 B_i^2) (A_i^2 B_i^2) + (A_i^2 B_i^2) (A_i^2 B_i^2) (A_i^2 B_i^2) + (A_i^2 B_i^2) (A_i^2 B_i^2) + (A_i^2 B_i^2) (A_i^2 B_i^2) (A_i^2 B_i^2) (A_i^2 B_i^2) + (A_i^2 B_i^2) (A_i^2 B_i^2) (A_i^2 B_i^2) (A_i^2 B_i^2) + (A_i^2 B_i^2) (A_i^2 B_i^2)$

 $C_{XY} = \frac{\{(F_{0}^{2}A_{1}B_{1})(A_{1}^{4}B_{1}^{4}) + (F_{0}^{2}B_{1}^{2})(A_{1}^{2}B_{1}) + (F_{0}^{2}A_{1}^{2})(A_{1}^{2}B_{1}) + (F_{0}^{2}A_{1}^{2})(A_{1}^{2}B_{1}) + (F_{0}^{2}A_{1}^{2})(A_{1}^{2}B_{1}^{2}) + (F_{0}^{2}A_{1}B_{1}^{2})(A_{1}^{2}B_{1}^{2}) + (F_{0}^{2}A_{1}B_{1}^{2})(A_{1}^{2}B_{1}^{2}) + (F_{0}^{2}A_{1}^{2})(B_{1}^{4}A_{1}^{2}B_{1}^{2}) + (F_{0}^{2}A_{1}^{2})(B_{1}^{4}A_{1}^{2}B_{1}^{2}) + (F_{0}^{2}A_{1}^{2}B_{1}^{2})(A_{1}^{2}B_{1}^{2}) + (F_{0}^{2}A_{1}^{2}B_{1}^{2})(A_{1}^{2}B_{1}^{2})(A_{1}^{2}B_{1}^{2}) + (F_{0}^{2}A_{1}^{2}B_{1}^{2})(A_{1}^{2}B_{1}^{2})(A_{1}^{2}B_{1}^{2}) + (F_{0}^{2}A_{1}^{2}B_{1}^{2})(A_{1}^{2}B_{1}^{2})(A_{1}^{2}B_{1}^{2}) + (F_{0}^{2}A_{1}^{2}B_{1}^{2})(A_{1}^{2}B_{1}^{2})(A_{1}^{2}B_{1}^{2}) + (F_{0}^{2}A_{1}^{2}B_{1}^{2})(A_{1}^{2}B_{1}^{2})(A_{1}^{2}B_{1}^{2}) + (F_{0}^{2}A_{1}^{2}B_{1}^{2})(A_{1}^{2}B_{1}^{2})(A_{1}^{2}B_{1}^{2}) + (F_{0}^{2}A_{1}^{2}B_{1}^{2})(A_{1}^{2}B_{1}$

For the special case where only one parameter was varied $(\Delta Y = 0)$, the equations reduce to

$$\delta X^2 = \frac{F_{0i}^2 A_i^2}{A_i^4} \quad \delta Y^2 = 0 \quad C_{XY} = 0$$
 (A.6a-c)

Substituting these values of δX^2 , δY^2 and C_{XY} in equation 5 will give the value of the predicted F_P .

References

Adegoke, O., Rakshit, S., Mukhopadhyay, B., 2017. Spectral and time series analyses of the seyfert 1 agn: Zw 229.015. Monthly Notices of the Royal Astronomical Society 466, 3951–3960.

Alston, W.N., Fabian, A.C., Kara, E., Parker, M.L., Dovciak, M., Pinto, C., Jiang, J., Middleton, M.J., Miniutti, G., Walton, D.J., et al., 2020. A dynamic black hole corona in an active galaxy through x-ray reverberation mapping. Nature Astronomy 4, 597–602.

- Arévalo, P., McHardy, I., Summons, D., 2008. X-ray variability of the seyfert 1 markarian 335: power spectrum and time lags. Monthly Notices of the Royal Astronomical Society 388, 211–218.
- Arnaud, K., 1996. Xspec: the first ten years, in: Astronomical data analysis software and systems V, p. 17.
- Arnaud, K., Branduardi-Raymont, G., Culhane, J., Fabian, A., Hazard, C., McGlynn, T., Shafer, R., Tennant, A., Ward, M., 1985. Exosat observations of a strong soft x-ray excess in mkn 841. Monthly Notices of the Royal Astronomical Society 217, 105–113.
- Bambi, C., 2024. Towards a new generation of reflection models for precision measurements of accreting black holes. arXiv preprint arXiv:2410.02251.
- Boissay, R., Ricci, C., Paltani, S., 2016. A hard x-ray view of the soft excess in agn. Astronomy & Astrophysics 588, A70.
- Boller, T., 2023. Unraveling the enigmatic soft x-ray excess: Current understanding and future perspectives. Astronomische Nachrichten 344, e230105.
- Boller, T., Brandt, W.N., Fink, H., 1995. Soft x-ray properties of 'narrow-line' seyfert 1 galaxies. arXiv preprint astro-ph/9504093.
- Brightman, M., Nandra, K., 2011. An xmm–newton spectral survey of 12 μ m selected galaxies–i. x-ray data. Monthly Notices of the Royal Astronomical Society 413, 1206–1235.
- Bühler, P., Courvoisier, T.L., Staubert, R., Brunner, H., Lamer, G., 1995. Rosat spectra of quasars. Astronomy and Astrophysics 295, 309–316.
- Chainakun, P., Young, A., 2015. Simultaneous spectral and reverberation modelling of relativistic reflection in mrk 335. Monthly Notices of the Royal Astronomical Society 452, 333–342.
- Chainakun, P., Young, A.J., Kara, E., 2016. Relativistic x-ray reverberation modelling of the combined time-averaged and lag-energy spectra in agn. Monthly Notices of the Royal Astronomical Society 460, 3076–3088.
- Chevallier, L., Collin, S., Dumont, A.M., Czerny, B., Mouchet, M., Gonçalves, A.C., Goosmann, R., 2006. The role of absorption and reflection in the soft x-ray excess of active galactic nuclei-i. preliminary results. Astronomy & Astrophysics 449, 493–508.
- Choudhury, K., Nampalliwar, S., Abdikamalov, A.B., Ayzenberg, D., Bambi, C., Dauser, T., García, J.A., 2019. Testing the kerr metric with x-ray reflection spectroscopy of mrk 335 suzaku data. The Astrophysical Journal 879, 80
- Crummy, J., Fabian, A., Gallo, L., Ross, R., 2006. An explanation for the soft x-ray excess in active galactic nuclei. Monthly Notices of the Royal Astronomical Society 365, 1067–1081.
- Dauser, T., García, J., Parker, M., Fabian, A., Wilms, J., 2014. The role of the reflection fraction in constraining black hole spin. Monthly Notices of the Royal Astronomical Society: Letters 444, L100–L104.
- Dauser, T., García, J., Parker, M., Fabian, A., Wilms, J., Lohfink, A., Kallman, T., Steiner, J., McClintock, J., Brenneman, L., et al., 2020. reixill: Reflection models of black hole accretion disks. Astrophysics Source Code Library, ascl–2010.
- Dauser, T., García, J., Walton, D., Eikmann, W., Kallman, T., McClintock, J., Wilms, J., 2016. Normalizing a relativistic model of x-ray reflectiondefinition of the reflection fraction and its implementation in relxill. Astronomy & Astrophysics 590, A76.
- De Marco, B., Ponti, G., Cappi, M., Dadina, M., Uttley, P., Cackett, E., Fabian, A., Miniutti, G., 2013. Discovery of a relation between black hole mass and soft x-ray time lags in active galactic nuclei. Monthly Notices of the Royal Astronomical Society 431, 2441–2452.
- Dewangan, G., Griffiths, R., Dasgupta, S., Rao, A., 2007. An investigation of the origin of soft x-ray excess emission from ark 564 and mrk 1044. The Astrophysical Journal 671, 1284.
- Ding, N., Gu, Q., Tang, Y., Xiong, D., Guo, X., Xu, X., Geng, X., Ge, X., Chen, Y., 2022. The variability and soft x-ray excess properties of narrowline seyfert 1 galaxies: The swift view. Astronomy & Astrophysics 659, A172
- Done, C., Davis, S., Jin, C., Blaes, O., Ward, M., 2012. Intrinsic disc emission and the soft x-ray excess in active galactic nuclei. Monthly Notices of the Royal Astronomical Society 420, 1848–1860.
- Done, C., Nayakshin, S., 2007. Can the soft excess in agn originate from disc reflection? Monthly Notices of the Royal Astronomical Society: Letters 377, L59–L63.
- Edelson, R., Krolik, J., Pike, G., 1990. Broad-band properties of the cfa seyfert galaxies. iii-ultraviolet variability. Astrophysical Journal, Part 1 (ISSN 0004-637X), vol. 359, Aug. 10, 1990, p. 86-97. 359, 86-97.
- Edelson, R., Turner, T., Pounds, K., Vaughan, S., Markowitz, A., Marshall,

- H., Dobbie, P., Warwick, R., 2002. X-ray spectral variability and rapid variability of the soft x-ray spectrum seyfert 1 galaxies arakelian 564 and ton s180. The Astrophysical Journal 568, 610.
- Emmanoulopoulos, D., Papadakis, I., Epitropakis, A., Pecháček, T., Dovčiak, M., McHardy, I., 2016. A search for x-ray reprocessing echoes in the power spectral density functions of agn. Monthly Notices of the Royal Astronomical Society 461, 1642–1655.
- Epitropakis, A., Papadakis, I., Dovčiak, M., Pecháček, T., Emmanoulopoulos, D., Karas, V., McHardy, I., 2016. Theoretical modelling of the agn iron line vs. continuum time-lags in the lamp-post geometry. Astronomy & Astrophysics 594 A71
- Ezhikode, S.H., Dewangan, G.C., Misra, R., 2021. Astrosat view of the nls1 galaxy mrk 335. Journal of Astrophysics and Astronomy 42, 51.
- Ezhikode, S.H., Dewangan, G.C., Misra, R., Tripathi, S., Philip, N.S., Kembhavi, A.K., 2016. Uv and x-ray variability of the narrow-line seyfert 1 galaxy ark 564. Research in Astronomy and Astrophysics 16, 008.
- Ezhikode, S.H., Gandhi, P., Done, C., Ward, M., Dewangan, G.C., Misra, R., Philip, N.S., 2017. Determining the torus covering factors for a sample of type 1 agn in the local universe. Monthly Notices of the Royal Astronomical Society 472, 3492–3511.
- Fabian, A., Iwasawa, K., Reynolds, C., Young, A., 2000. Broad iron lines in active galactic nuclei. Publications of the Astronomical Society of the Pacific 112, 1145.
- Fabian, A.C., Zoghbi, A., Ross, R., Uttley, P., Gallo, L., Brandt, W., Blustin, A., Boller, T., Caballero-Garcia, M., Larsson, J., et al., 2009. Broad line emission from iron k-and l-shell transitions in the active galaxy 1h 0707-495. Nature 459, 540–542.
- Gallo, L., Blue, D., Grupe, D., Komossa, S., Wilkins, D., 2018. Eleven years of monitoring the seyfert 1 mrk 335 with swift: Characterizing the x-ray and uv/optical variability. Monthly Notices of the Royal Astronomical Society 478, 2557–2568.
- Gallo, L., Gonzalez, A., Waddell, S., Ehler, H., Wilkins, D., Longinotti, A., Grupe, D., Komossa, S., Kriss, G., Pinto, C., et al., 2019. Evidence for an emerging disc wind and collimated outflow during an x-ray flare in the narrow-line seyfert 1 galaxy mrk 335. Monthly Notices of the Royal Astronomical Society 484, 4287–4297.
- Gallo, L.C., Fabian, A., Grupe, D., Bonson, K., Komossa, S., Longinotti, A., Miniutti, G., Walton, D., Zoghbi, A., Mathur, S., 2013. A blurred reflection interpretation for the intermediate flux state in mrk 335. Monthly Notices of the Royal Astronomical Society 428, 1191–1200.
- Gallo, L.C., Miniutti, G., Miller, J., Brenneman, L., Fabian, A., Guainazzi, M., Reynolds, C., 2011. Multi-epoch x-ray observations of the seyfert 1.2 galaxy mrk 79: bulk motion of the illuminating x-ray source. Monthly Notices of the Royal Astronomical Society 411, 607–619.
- Gallo, L.C., Wilkins, D., Bonson, K., Chiang, C.Y., Grupe, D., Parker, M., Zoghbi, A., Fabian, A., Komossa, S., Longinotti, A., 2015. Suzaku observations of mrk 335: confronting partial covering and relativistic reflection. Monthly Notices of the Royal Astronomical Society 446, 633–650.
- García, J., Dauser, T., Lohfink, A., Kallman, T., Steiner, J., McClintock, J., Brenneman, L., Wilms, J., Eikmann, W., Reynolds, C., et al., 2014. Improved reflection models of black hole accretion disks: treating the angular distribution of x-rays. The Astrophysical Journal 782, 76.
- García, J.A., Kara, E., Walton, D., Beuchert, T., Dauser, T., Gatuzz, E., Balokovic, M., Steiner, J.F., Tombesi, F., Connors, R.M., et al., 2019. Implications of the warm corona and relativistic reflection models for the soft excess in mrk 509. The Astrophysical Journal 871, 88.
- Gliozzi, M., Williams, J.K., 2020. The soft x-ray excess: Nls1s versus bls1s. Monthly Notices of the Royal Astronomical Society 491, 532–543.
- Green, A.R., McHardy, I., Lehto, H., 1993. On the nature of rapid x-ray variability in active galactic nuclei. Monthly Notices of the Royal Astronomical Society 265, 664–680.
- Grier, C., Peterson, B., Pogge, R., Denney, K., Bentz, M., Martini, P., Sergeev, S., Kaspi, S., Zu, Y., Kochanek, C., et al., 2011. A reverberation lag for the high-ionization component of the broad-line region in the narrow-line seyfert 1 mrk 335. The Astrophysical Journal Letters 744, L4.
- Grupe, D., Komossa, S., Gallo, L.C., 2007. Discovery of the narrow-line seyfert 1 galaxy markarian 335 in a historical low x-ray flux state. The Astrophysical Journal 668, L111.
- Grupe, D., Komossa, S., Gallo, L.C., Fabian, A.C., Larsson, J., Pradhan, A.K., Xu, D., Miniutti, G., 2008. Xmm-newton observations of the narrow-line seyfert 1 galaxy mrk 335 in a historical low x-ray flux state. The Astrophys-

- ical Journal 681, 982.
- Hancock, S., Young, A., Chainakun, P., 2022. X-ray timing and spectral analysis of reverberating active galactic nuclei. Monthly Notices of the Royal Astronomical Society 514, 5403–5421.
- Huchra, J.P., Vogeley, M.S., Geller, M.J., 1999. The cfa redshift survey: Data for the south galactic cap*. The Astrophysical Journal Supplement Series 121, 287
- Ingram, A., 2019. Error formulae for the energy-dependent cross-spectrum. Monthly Notices of the Royal Astronomical Society 489, 3927–3938.
- Ingram, A., Mastroserio, G., Dauser, T., Hovenkamp, P., van der Klis, M., García, J.A., 2019. A public relativistic transfer function model for x-ray reverberation mapping of accreting black holes. Monthly Notices of the Royal Astronomical Society 488, 324–347.
- Iso, N., Ebisawa, K., Sameshima, H., Mizumoto, M., Miyakawa, T., Inoue, H., Yamasaki, H., 2016. Origin of the broad iron line feature and the soft x-ray variation in seyfert galaxies. Publications of the Astronomical Society of Japan 68, S27.
- Jansen, F., Lumb, D., Altieri, B., Clavel, J., Ehle, M., Erd, C., Gabriel, C., Guainazzi, M., Gondoin, P., Much, R., et al., 2001. Xmm-newton observatory-i. the spacecraft and operations. Astronomy & Astrophysics 365, L1–L6.
- Kalberla, P.M., Burton, W., Hartmann, D., Arnal, E.M., Bajaja, E., Morras, R., Pöppel, W.G., 2005. The leiden/argentine/bonn (lab) survey of galactic hi-final data release of the combined lds and iar surveys with improved strayradiation corrections. Astronomy & Astrophysics 440, 775–782.
- Kara, E., Fabian, A., Cackett, E., Uttley, P., Wilkins, D., Zoghbi, A., 2013. Discovery of high-frequency iron k lags in ark 564 and mrk 335. Monthly Notices of the Royal Astronomical Society 434, 1129–1137.
- Keek, L., Ballantyne, D., 2016. Revealing the accretion disc corona in mrk 335 with multi-epoch x-ray spectroscopy. Monthly Notices of the Royal Astronomical Society 456, 2722–2734.
- Komossa, S., Grupe, D., Gallo, L., Poulos, P., Blue, D., Kara, E., Kriss, G., Longinotti, A., Parker, M., Wilkins, D., 2020. Lifting the curtain: The seyfert galaxy mrk 335 emerges from deep low-state in a sequence of rapid flare events. Astronomy & Astrophysics 643, L7.
- Komossa, S., Grupe, D., Schartel, N., Gallo, L., Gomez, J., Kollatschny, W., Kriss, G., Leighly, K., Longinotti, A., Parker, M., et al., 2016. The extremes of agn variability. Proceedings of the International Astronomical Union 12, 168–171.
- Kubota, A., Done, C., 2018. A physical model of the broad-band continuum of agn and its implications for the uv/x relation and optical variability. Monthly Notices of the Royal Astronomical Society 480, 1247–1262.
- Larsson, J., Miniutti, G., Fabian, A., Miller, J., Reynolds, C., Ponti, G., 2008. Suzaku observations of markarian 335: evidence for a distributed reflector. Monthly Notices of the Royal Astronomical Society 384, 1316–1326.
- Lawrence, A., Papadakis, I., 1993. X-ray variability of active galactic nuclei-a universal power spectrum with luminosity-dependent amplitude. The Astrophysical Journal 414, L85–L88.
- Lawrence, A., Watson, M., Pounds, K., Elvis, M., 1987. Low-frequency divergent x-ray variability in the seyfert galaxy ngc4051. Nature 325, 694–696.
- Liebmann, A.C., Fabian, A.C., Tsuruta, S., Haba, Y., Kunieda, H., 2018. X-ray spectral properties of seyfert i galaxy leda 168563. The Astrophysical Journal 868, 11.
- Liu, H., Luo, B., Brandt, W., Brotherton, M.S., Gallagher, S., Ni, Q., Shemmer, O., Timlin, J., 2021a. On the observational difference between the accretion disk-corona connections among super-and sub-eddington accreting active galactic nuclei. The Astrophysical Journal 910, 103.
- Liu, H., Parker, M., Jiang, J., Kara, E., Bambi, C., Grupe, D., Komossa, S., 2021b. A systematic study of photoionized emission and warm absorption signatures of the nls1 mrk 335. Monthly Notices of the Royal Astronomical Society 506, 5190–5200.
- Liu, T., Wang, J.X., 2010. The difference in narrow fe $k\alpha$ line emission between seyfert 1 and seyfert 2 galaxies. The Astrophysical Journal 725, 2381.
- Longinotti, A., Krongold, Y., Kriss, G., Ely, J., Gallo, L., Grupe, D., Komossa, S., Mathur, S., Pradhan, A., 2013. The rise of an ionized wind in the narrow-line seyfert 1 galaxy mrk 335 observed by xmm-newton and hst. The Astrophysical Journal 766, 104.
- Longinotti, A., Nucita, A., Santos-Lleo, M., Guainazzi, M., 2008. The seyfert 1 galaxy mrk 335 at a very low flux state: mapping the soft x-ray photoionised gas. Astronomy & Astrophysics 484, 311–315.
- Longinotti, A.L., Sim, S., Nandra, K., Cappi, M., 2007. Evidence for relativistic

- features in the x-ray spectrum of mrk 335. Monthly Notices of the Royal Astronomical Society 374, 237–247.
- Markowitz, A., Edelson, R., Vaughan, S., 2003. Long-term x-ray spectral variability in seyfert 1 galaxies. The Astrophysical Journal 598, 935.
- Marshall, N., Warwick, R., Pounds, K., 1981. The variability of x-ray emission from active galaxies. Monthly Notices of the Royal Astronomical Society 194, 987–1002.
- Martin Gaskell, C., Klimek, E.S., 2003. Variability of active galactic nuclei from the optical to x-ray regions. Astronomical & Astrophysical Transactions 22, 661–679.
- Mastroserio, G., Ingram, A., van Der Klis, M., 2020. Multi-timescale reverberation mapping of mrk 335. Monthly Notices of the Royal Astronomical Society 498, 4971–4982.
- Matzeu, G., Nardini, E., Parker, M., Reeves, J., Braito, V., Porquet, D., Middei, R., Kammoun, E., Lusso, E., Alston, W., et al., 2020. The first broad-band x-ray view of the narrow-line seyfert 1 ton s180. Monthly Notices of the Royal Astronomical Society 497, 2352–2370.
- McHardy, I., 1985. X-ray timing and spectral observations of active galactic nuclei. Space Science Reviews 40, 559–584.
- McHardy, I., 1988. Exosat observations of variability in active galactic nuclei. Società Astronomica Italiana, Memorie (ISSN 0037-8720), vol. 59, no. 1-2, 1988, p. 239-259. 59, 239-259.
- Middei, R., Bianchi, S., Cappi, M., Petrucci, P.O., Ursini, F., Arav, N., Behar, E., Branduardi-Raymont, G., Costantini, E., De Marco, B., et al., 2018. Multi-wavelength campaign on ncg 7469-iv. the broad-band x-ray spectrum. Astronomy & Astrophysics 615, A163.
- Middei, R., Bianchi, S., Petrucci, P., Ursini, F., Cappi, M., De Marco, B., De Rosa, A., Malzac, J., Marinucci, A., Matt, G., et al., 2019. High-energy monitoring of ngc 4593 ii. broad-band spectral analysis: testing the twocorona model. Monthly Notices of the Royal Astronomical Society 483, 4695–4705.
- Middei, R., Petrucci, P.O., Bianchi, S., Ursini, F., Cappi, M., Clavel, M., De Rosa, A., Marinucci, A., Matt, G., Tortosa, A., 2020. The soft excess of the nls1 galaxy mrk 359 studied with an xmm-newton-nustar monitoring campaign. Astronomy & Astrophysics 640, A99.
- Middleton, M., Done, C., Gierliński, M., 2007. An absorption origin for the soft excess in seyfert 1 active galactic nuclei. Monthly Notices of the Royal Astronomical Society 381, 1426–1436.
- Middleton, M., Done, C., Ward, M., Gierliński, M., Schurch, N., 2009. Re j1034+ 396: the origin of the soft x-ray excess and quasi-periodic oscillation. Monthly Notices of the Royal Astronomical Society 394, 250–260.
- Miniutti, G., Fabian, A., 2004. A light bending model for the x-ray temporal and spectral properties of accreting black holes. Monthly Notices of the Royal Astronomical Society 349, 1435–1448.
- Nandra, K., 2001. X-ray variability of agn and correlations with spectral properties. Advances in Space Research 28, 295–306.
- Nandra, K., Pounds, K., 1994. Ginga observations of the x-ray spectra of seyfert galaxies. Monthly Notices of the Royal Astronomical Society 268, 405–429.
- Newville, M., Stensitzki, T., Allen, D.B., Rawlik, M., Ingargiola, A., Nelson, A., 2016. Lmfit: Non-linear least-square minimization and curve-fitting for python. Astrophysics Source Code Library, ascl–1606.
- Noda, H., Done, C., 2018. Explaining changing-look agn with state transition triggered by rapid mass accretion rate drop. Monthly Notices of the Royal Astronomical Society 480, 3898–3906.
- O'Neill, P.M., Nandra, K., Cappi, M., Longinotti, A.L., Sim, S.A., 2007. On the relativistic iron line and soft excess in the seyfert 1 galaxy markarian 335. Monthly Notices of the Royal Astronomical Society: Letters 381, L94–L98.
- Page, K.L., Reeves, J., O'Brien, P.T., Turner, M.J., 2005. Xmm-newton spectroscopy of high-redshift quasars. Monthly Notices of the Royal Astronomical Society 364, 195–207.
- Papadakis, I., Binas-Valavanis, V., 2024. The x-ray variability of agn: power-spectrum and variance analysis of the swift/bat light curves. arXiv preprint arXiv:2402.15373.
- Parker, M., Longinotti, A., Schartel, N., Grupe, D., Komossa, S., Kriss, G., Fabian, A.C., Gallo, L., Harrison, F., Jiang, J., et al., 2019. The nuclear environment of the nls1 mrk 335: Obscuration of the x-ray line emission by a variable outflow. Monthly Notices of the Royal Astronomical Society 490, 683–697.
- Parker, M., Wilkins, D., Fabian, A., Grupe, D., Dauser, T., Matt, G., Harrison, F., Brenneman, L., Boggs, S., Christensen, F.E., et al., 2014. The nustar spectrum of mrk 335: extreme relativistic effects within two gravitational

- radii of the event horizon? Monthly Notices of the Royal Astronomical Society 443, 1723–1732.
- Patrick, A., Reeves, J., Porquet, D., Markowitz, A., Lobban, A., Terashima, Y., 2011. Iron line profiles in suzaku spectra of bare seyfert galaxies. Monthly Notices of the Royal Astronomical Society 411, 2353–2370.
- Petrucci, P.O., Ursini, F., De Rosa, A., Bianchi, S., Cappi, M., Matt, G., Dadina, M., Malzac, J., 2018. Testing warm comptonization models for the origin of the soft x-ray excess in agns. Astronomy & Astrophysics 611, A59.
- Porquet, D., Reeves, J., Matt, G., Marinucci, A., Nardini, E., Braito, V., Lobban, A., Ballantyne, D., Boggs, S., Christensen, F.E., et al., 2018. A deep x-ray view of the bare agn ark 120-iv. xmm-newton and nustar spectra dominated by two temperature (warm, hot) comptonization processes. Astronomy & Astrophysics 609, A42.
- Pounds, K., Stanger, V., Turner, T., King, A., Czerny, B., 1987. Discovery of a strong soft x-ray excess in mkn 335-evidence for an accretion disc? Monthly Notices of the Royal Astronomical Society 224, 443-452.
- Pryal, M., Falcone, A., Stroh, M., 2015. A search for fast x-ray variability from active galactic nuclei using swift. The Astrophysical Journal 802, 33.
- Reeves, J., Done, C., Pounds, K., Terashima, Y., Hayashida, K., Anabuki, N., Uchino, M., Turner, M., 2008. On why the iron k-shell absorption in agn is not a signature of the local warm/hot intergalactic medium. Monthly Notices of the Royal Astronomical Society: Letters 385, L108–L112.
- Reynolds, C.S., 2021. Observational constraints on black hole spin. Annual Review of Astronomy and Astrophysics 59, 117–154.
- Rodriguez-Pascual, P., Alloin, D., Clavel, J., Crenshaw, D.M., Horne, K., Kriss, G.A., Krolik, J.H., Malkan, M.A., Netzer, H., O'Brien, P.T., et al., 1997. Steps toward determination of the size and structure of the broad-line region in active galactic nuclei. ix. ultraviolet observations of fairall 9. The Astrophysical Journal Supplement Series 110, 9.
- Sarma, R., Tripathi, S., Misra, R., Dewangan, G., Pathak, A., Sarma, J., 2015. Relationship between x-ray spectral index and x-ray eddington ratio for mrk 335 and ark 564. Monthly Notices of the Royal Astronomical Society 448, 1541–1550.
- Serafinelli, R., De Rosa, A., Tortosa, A., Stella, L., Vagnetti, F., Bianchi, S., Ricci, C., Kammoun, E., Petrucci, P.O., Middei, R., et al., 2024. Investigating the interplay between agn coronal properties and hard x-ray variability with nustar. arXiv preprint arXiv:2407.06769.
- Singh, K., Garmire, G., Nousek, J., 1985. Observations of soft x-ray spectrum from a seyfert 1 and a narrow emission-line galaxy. The Astrophysical Journal 297, 633–638.
- Sobolewska, M., Done, C., 2005. What is the origin of the soft excess in agn?, in: AIP Conference Proceedings, AIP. p. 317–319. URL: http://dx.doi.org/10.1063/1.1960944, doi:10.1063/1.1960944.
- Soldi, S., Beckmann, V., Baumgartner, W.H., Ponti, G., Shrader, C.R., Lubiński, P., Krimm, H., Mattana, F., Tueller, J., 2014. Long-term variability of agn at hard x-rays. Astronomy & Astrophysics 563, A57.
- Steiner, J.F., Narayan, R., McClintock, J.E., Ebisawa, K., 2009. A simple comptonization model. Publications of the Astronomical Society of the Pacific 121, 1279.
- Strüder, L., Briel, U., Dennerl, K., Hartmann, R., Kendziorra, E., Meidinger, N., Pfeffermann, E., Reppin, C., Aschenbach, B., Bornemann, W., et al., 2001. The european photon imaging camera on xmm-newton: the pn-ccd camera. Astronomy & Astrophysics 365, L18–L26.
- Tanaka, Y., Boller, T., Gallo, L., Keil, R., Ueda, Y., 2004. Partial covering interpretation of the x-ray spectrum of the nls1 1h 0707- 495. Publications of the Astronomical Society of Japan 56, L9–L13.
- Tatum, M., Turner, T., Sim, S.A., Miller, L., Reeves, J., Patrick, A., Long, K., 2012. Modeling the fe k line profiles in type i active galactic nuclei with a compton-thick disk wind. The Astrophysical Journal 752, 94.
- Tombesi, F., Cappi, M., Reeves, J., Palumbo, G., Yaqoob, T., Braito, V., Dadina, M., 2010. Evidence for ultra-fast outflows in radio-quiet agns-i. detection and statistical incidence of fe k-shell absorption lines. Astronomy & Astrophysics 521, A57.
- Tripathi, S., Waddell, S., Gallo, L., Welsh, W., Chiang, C., 2019. The nature of the soft excess and spectral variability in the seyfert 1 galaxy zw 229.015. Monthly Notices of the Royal Astronomical Society 488, 4831–4842.
- Turner, T., George, I., Nandra, K., Turcan, D., 1999. On x-ray variability in seyfert galaxies. The Astrophysical Journal 524, 667.
- Turner, T., George, I., Netzer, H., 1996. Complex absorption in the Seyfert 1 galaxy EXO 055620-3820.2. Technical Report. SCAN-9605049.
- Turner, T., Pounds, K., 1988. Variability of the soft excess in the seyfert i

- galaxy mkn 335. Monthly Notices of the Royal Astronomical Society 232, 463–471.
- Turner, T.J., 1994. X-ray variability in agn, in: The Nature of Compact Objects in Active Galactic Nuclei: Proceedings of the 33rd Herstmonceux Conference, Held in Cambridge, July 6-22, 1992, Cambridge University Press. p. 257.
- Ursini, F., Petrucci, P.O., Bianchi, S., Matt, G., Middei, R., Marcel, G., Ferreira, J., Cappi, M., De Marco, B., De Rosa, A., et al., 2020. Nustar/xmm-newton monitoring of the seyfert 1 galaxy he 1143-1810-testing the two-corona scenario. Astronomy & Astrophysics 634, A92.
- Vaughan, S., Edelson, R., Warwick, R., Uttley, P., 2003. On characterizing the variability properties of x-ray light curves from active galaxies. Monthly Notices of the Royal Astronomical Society 345, 1271–1284.
- Weaver, K., Mushotzky, R., Arnaud¹, K., Serlemitsos, P., Marshall, F., Petre, R., Jahoda, K., Smale, A., Netzer, H., Branch, X.r.A., 1993. The complex soft x-ray excess in ngc 4151, in: BBXRT: A Preview to Astronomical X-ray Spectroscopy in the 90's: Journal Papers and Selected Conference Contributions, Laboratory for High Energy Astrophysics, NASA/Goddard Space Flight Center. p. 477.
- Wilkins, D., Gallo, L.C., 2015. Driving extreme variability: the evolving corona and evidence for jet launching in markarian 335. Monthly Notices of the Royal Astronomical Society 449, 129–146.
- Wilkins, D., Gallo, L.C., Grupe, D., Bonson, K., Komossa, S., Fabian, A., 2015. Flaring from the supermassive black hole in mrk 335 studied with swift and nustar. Monthly Notices of the Royal Astronomical Society 454, 4440–4451.
- Yamasaki, H., Mizumoto, M., Ebisawa, K., Sameshima, H., 2016. Origin of the characteristic x-ray spectral variations of iras 13224-3809. Publications of the Astronomical Society of Japan 68, 80.
- Yang, H., Jin, C., Yuan, W., 2022. Exploring the link between the x-ray power spectra and energy spectra of active galactic nuclei. The Astrophysical Journal 936, 36.
- Yu, Z., Jiang, J., Bambi, C., Gallo, L.C., Grupe, D., Fabian, A.C., Reynolds, C.S., Brandt, W.N., 2023. An xmm-newton study of six narrow-line seyfert 1 galaxies at z= 0.35-0.92. Monthly Notices of the Royal Astronomical Society 522, 5456-5468.
- Zhong, X., Wang, J., 2013. A magnetic reconnection origin for the soft x-ray excess in an active galactic nucleus. The Astrophysical Journal 773, 23.
- Zoghbi, A., Miller, J., 2023. Measuring the soft excess region size relative to the corona in active galactic nuclei with nicer. The Astrophysical Journal 957, 69.